Analytical Science Advances

Chemistry Europe
European Chemical Societies Publishing

RESEARCH ARTICLE OPEN ACCESS

A Selective Phenyl Azo Acetate Substrate for Enhanced Carbonic Anhydrase Functional Analysis

Justinas Babinskas | Inga Matijošytė

Sector of Applied Biocatalysis, Institute of Biotechnology, Vilnius University Life Sciences Center, Vilnius, Lithuania

Correspondence: Inga Matijošytė (inga.matijosyte@bti.vu.lt)

Received: 22 January 2026 | **Revised:** 17 April 2026 | **Accepted:** 28 April 2026

ABSTRACT

Carbon dioxide (CO_2) sequestration is a key strategy for mitigating climate change, and biocatalytic approaches offer sustainable, cost-effective alternatives to chemical and physical methods. Carbonic anhydrases (CAs) efficiently catalyse the reversible hydration of CO_2 to bicarbonate, yet their large-scale application is constrained by limited stability and the lack of robust analytical tools for activity and/or inhibition profiling. In this work, we synthesised and characterised a novel phenyl azo dye acetate to address these limitations. The substrate was optimised for spectrophotometric assays, enabling reliable kinetic and inhibition analyses of CAs. Compared with conventional substrates such as *p*-nitrophenyl acetate and indoxyl acetate, the new assay demonstrated more than 4.5-fold higher sensitivity, substantial thermal stability and wider applicability across tested hydrolases. These findings provide a more robust platform for evaluating CA activity, supporting the development of more efficient biocatalytic systems for CO_2 sequestration.

1 | Introduction

Carbonic anhydrases (CA) are a family of metalloenzymes (E.C. 4.2.1.1) which catalyse a reversible CO_2 hydration to bicarbonate ion (HCO_3^-) and proton (H^+) [1]. This apparently simple reaction plays a central role in acid–base homeostasis, respiration, photosynthesis and CO_2 transport across all domains of life [2]. The broad distribution of CAs in nature reflects their fundamental importance in both physiology and environmental adaptation [3]. Based on evolutionary origin and structural motifs, CAs are grouped into at least eight distinct families: α, β, γ, δ, ζ, η, θ and ι. Among these, the α-CAs are predominant in vertebrates, with 16 isoforms described in humans. These isoforms are of special interest for biomedical research as they participate in diverse metabolic processes, including renal acid–base regulation, bone resorption, lipogenesis and neural signalling [2, 4]. In addition to their biomedical roles, CAs have gained attention in industrial biotechnology and environmental applications. The hydration of CO_2 catalysed by CAs is one of the fastest enzymatic reactions known, with turnover rates in the order of 10^6 M^{-1} s^{-1} [2, 5]. This remarkable catalytic efficiency makes CAs attractive candidates for CO_2 capture and sequestration technologies [6–8]. However, the practical application of CAs in industrial processes remains limited by challenges such as enzyme instability at elevated temperatures, denaturing solvents and the alkaline conditions typical of capture processes [9]. Strategies including enzyme immobilisation on solid supports [10] and the use of non-conventional solvents [11] have been explored; yet, one of the persistent bottlenecks in the pipeline development is the lack of robust, high-throughput and physiologically relevant assays for CA activity.

Functional characterisation of enzymes relies heavily on the ability to monitor the conversion of substrates into products. For CAs, assay development is complicated by the gaseous nature of the physiological substrate (CO_2) and the ultrafast catalytic rates. The earliest widely adopted method, described by Wilbur and Anderson [12], is a potentiometric assay that monitors pH changes during CO_2 hydration in water. While historically important, this method suffers from limitations including variable

CO_2 solubility, dependence on electrode response time and poor suitability for high-throughput applications. Today, the stopped-flow spectrophotometric assay is considered the gold standard, as it directly measures the hydration of CO_2 with millisecond resolution, enabling accurate determination of turnover numbers in the physiological range [13, 14]. This technique, however, requires specialised instrumentation and is not always accessible for routine, large-scale or environmental non-pure sample screening. Because of these constraints, alternative substrates and so-called surrogate reactions have been employed to probe CA activity. One of the most useful properties of CAs is their esterase activity, first described in the 1960s [15]. This activity can be monitored by using chromogenic esters such as *p*-nitrophenyl acetate (*p*-NPA), which release a coloured product upon hydrolysis and can be quantified by spectrophotometry [16]. The *p*-NPA assay is inexpensive, straightforward and adaptable to multiwell plate formats, making it widely used in both basic CA research and inhibitor screening [17]. However, not all CAs expose esterase activity. Despite its convenience, *p*-NPA also presents drawbacks. It has limited water solubility, is prone to autohydrolysis and exhibits substrate promiscuity, as its hydrolysis is catalysed by many other hydrolases, including chymotrypsin [18], trypsin, carboxylesterases [19], hydroxynitrile lyases [20], lipases [21] and other esterases [22]. Additional complications arise when some substrates contain sulfonic acid groups, as these are known zinc-binding motifs that act as CA inhibitors [1]. In such cases, the substrate itself may partially inhibit the enzyme, complicating the interpretation of kinetic and inhibition data [23]. These issues highlight the urgent need for reliable and selective substrates for spectrophotometric assays to accurately characterise CA activity and/or inhibition.

To overcome these limitations, we explored a set of novel phenyl azo dye derivatives as potential chromogenic substrates for CA esterase assays. One promising candidate was synthesised via acetylation, characterised and evaluated for its spectrophotometric properties. The substrate was tested in an enzymatic assay, validated through inhibition studies and compared against standard CA esterase substrates such as *p*-NPA. Together, these developments advance more reliable tools for studying CA applications.

2 | Materials and Methods

2.1 | Materials

Across Organics: *p*-nitrophenol (*p*-NP); sodium nitrite; sodium sulfanilate hydrate; sodium hydroxide (NaOH); 5-aminoisophthalic acid; 2-propanol; acetic anhydride (Ac_2O); *N*,*N*-dimethylformamide (DMF); *N*-(2-hydroxyethyl)piperazine-*N*'-2-ethanesulfonic acid (HEPES); phosphoric acid; indoxyl acetate (indoxyl-Ac). *Merck*: concentrated hydrochloric acid (HCl), 36%–38%; potassium dihydrogen phosphate; sodium acetate; dipotassium hydrogen phosphate; sodium chloride; sodium dihydrogen phosphate dihydrate; disodium hydrogen phosphate dodecahydrate. *Fluka*: phenol; diethanolamine ($(EtOH)_2NH$); imidazole; gum arabic. *Sigma-Aldrich*: esterase from *Bacillus subtilis;* dimethyl sulfoxide (DMSO); α-bovine carbonic anhydrase II (bCAII); bovine serum albumin (BSA); *p*-NPA; *p*-nitrophenyl palmitate (*p*-NPP). *Chempur*: potassium hydroxide (KOH). *Thermo Scientific*: sodium succinate hexahydrate; tris(hydroxymethyl)aminomethane (TRIS); 5-acetamido-1,3,4-thiadiazole-2-sulfonamide (Acetazolamide). *P-L Biochemicals*: 1,3-amino-2-methyl-2-propanediol (AMPD). *Roth*: boric acid. *Chemapol*: potassium cyanide (KCN). *Serva*: Coomassie Brilliant Blue G-250. *Mavis*: ethanol (EtOH). *Fisher Scientific*: sodium salt deoxycholic acid. *Novozymes*: Lipolase 100 L; Finizym 250 L. *Biorro*: lipase LPS L.

CAs were kindly donated by Dr. Lina Baranauskienė and PhD student Tautvydas Kojis: (i) human carbonic anhydrase IX (hCAIX); *Pseudomonas aeruginosa* carbonic anhydrase 1 (psCA1) and 2 (psCA2).

Before activity measurements, enzymes were diluted to concentrations of 34.4 μM. A solution of BSA was prepared by dissolving 10 mg of protein powder in 1 mL of dH_2O. The concentration was measured using the Bradford assay and adjusted to 34.4 μM, based on a molecular mass of 66.4 kDa. Commercially available esterase from *B. subtilis* was prepared by dissolving 1 mg of enzyme powder in 1 mL of dH_2O and adjusting the final concentration to 3.44 μM, based on a molecular mass of 54.1 kDa. Lipolase 100L was diluted four times and lipase LPS L eight times for measurements with HABSA-Ac. The lipases were diluted 40- and 80-fold for esterase activity assays (*p*-NPA and indoxyl-Ac, respectively). Finizym 250 L was diluted four times for all activity measurements. Lipase-type activities for these three enzymes were measured using a *p*-NPP assay (see Supporting Information).

2.2 | Synthesis of Dyes and Substrate

The 4-(4-hydroxyphenylazo)benzenesulfonic acid (HABSA) synthesis (Scheme 1) was adapted from the work of Tang et al. [24]. In short, the main differences from the original article were these: the sulfanilic acid was substituted with 4.62 g (20 mmol) of sodium sulfanilate hydrate; the phenol amount was adjusted to 1.92 g (20.4 mmol); and the recrystallisation solvent was changed to dH_2O. Yield: 4.26 g (76.7%). Melting point: 282°C–287°C decomposed (lit. 282°C–285°C decompose). ^{1}H NMR (400 MHz, d_6-DMSO) δ (ppm): 10.35 (s, 1H), 7.82 (d, 2H, *J* 8.8 Hz), 7.77 (s, 4H), 6.95 (d, 2H, *J* 8.8 Hz). ^{13}C NMR (100 MHz, d_6-DMSO) δ (ppm): 161.5, 151.80, 149.85, 145.25, 126.64, 124.94, 121.60, 115.98. ATR-FTIR (cm^{-1}): 3585, 3502, 3288, 3018, 1619, 1590, 1499, 1461, 1432, 1391, 1363, 1269, 1247, 1184, 1146, 1118, 1101, 1034, 1002, 956, 893, 843, 794, 710, 621, 562, 526, 423.

The 5-(4-hydroxyphenylazo)isophthalic acid (HPDIA) synthesis followed a method analogous to that of HABSA. In this process, sodium sulfanilate hydrate was substituted with 3.67 g (20 mmol) of 5-aminoisophthalic acid. Product recrystallisation was performed in a 2-propanol: H_2O (1:4 v/v) mixture. The synthesis yield: 3.50 g (61.2%). Melting point: 282°C–287°C decomposed. ^{1}H NMR (400 MHz, d_6-DMSO) δ (ppm): 13.53 (s, 2H), 10.47 (s, 1H), 8.54 (s, 1H), 8.50 (s, 2H), 7.89 (d, 2H, *J* 8.4 Hz), 6.97 (d, 2H, *J* 8.4 Hz). ^{13}C NMR (100 MHz, d_6-DMSO) δ (ppm): 166.10, 161.76, 152.27, 145.08, 132.61, 130.92, 126.27, 125.43, 116.09. ATR-FTIR (cm^{-1}): 3332, 3082, 2954, 2821, 2575, 2515, 1698, 1650, 1606, 1586, 1504, 1475, 1457, 1418, 1311, 1269, 1243, 1216, 1188, 1147, 1109, 978, 918, 835, 804, 785, 758, 739, 871, 661, 842, 606, 561, 506, 476.

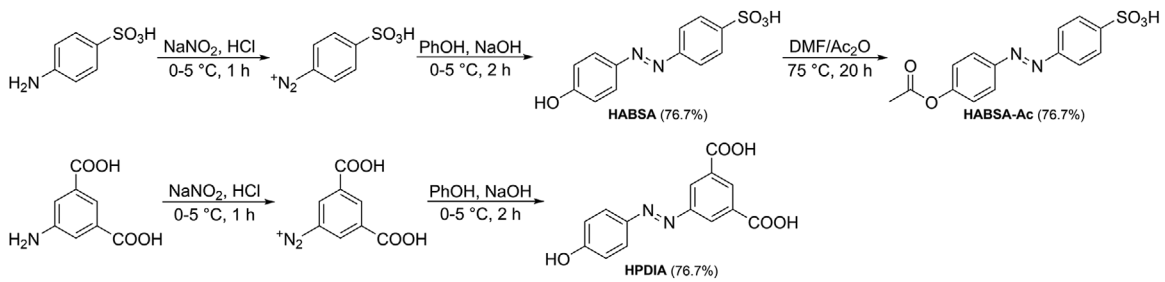

SCHEME 1 | Synthesis pathways for dyes and substrate.

The synthesis of 4-(4-acetoxyphenylazo) benzenesulfonic acid (HABSA-Ac) was adapted from Larsen et al. [25]. In summary, 0.52 g (1.83 mmol) of acid form of HABSA was used with 140 mL of a mixture of DMF and acetic anhydride (1:6). The reaction was then performed at 75°C for 20 h. The precipitate of the crude product was then washed with water (2 × 50 mL) and ethanol (2 × 50 mL). Yield: 0.367 g (70.6%). Melting point: 198°C–204°C (decomposed). ^{1}H NMR (400 MHz, d_6-DMSO) δ (ppm): 7.96 (dt, 2H, *J* 8.8 Hz, 2.8 Hz), 7.84 (qd, 4H, *J* 8.4 Hz, 2 Hz), 7.37 (dt, 2H, *J* 8.8 Hz, 2 Hz), 2.31 (s, 3H).^{13}C NMR (100 MHz, d_6-DMSO) δ (ppm): 169.11, 152.92, 151.66, 150.75, 149.62, 126.84, 123.95, 123.05, 122.24, 20.98. ATR-FTIR (cm^{-1}): 3101, 3063, 1763, 1593, 1488, 1368, 1302, 1235, 1183, 1153, 1127, 1102, 1048, 1008, 916, 852, 790, 726, 705, 661, 637, 615, 594, 575, 566, 530, 501.

2.3 | Characterisation of Dyes and Substrate

Determination of pK_{a2} for HABSA: The pK_{a2} of the dye HABSA was determined by potentiometric titration using a pH meter (Mettler Toledo SevenEasy S20) and a conductivity meter (Mettler Toledo SevenCompact S230). A 5 mM HABSA solution was prepared by dissolving 0.139 g of the dye in 100 mL of Milli-Q H_2O. Titration was performed using a burette with 0.1 M KOH solution. Stable pH and conductivity value measurements were recorded for each 0.1 mL of 0.1 M KOH added.

UV–vis spectra for HABSA: The absorption maxima (λ_{max}) of HABSA were measured at different pH values. Stock 5 mM HABSA stock solution was prepared by dissolving 0.139 g of dye in 100 mL of DMSO. Note that, 16.7 µM HABSA solutions for spectral measurements were prepared by diluting the stock solution with corresponding 50 mM concentration buffers at pH 3.0 (K-phosphate), 4.0 (Na-succinate), 5.0 (Na-acetate), 6.0 (K-phosphate), 7.0 (HEPES-HCl), 8.0 (HEPES-HCl), 8.5 (Tris–HCl), 9.0 (ethanolamine-HCl). UV-VIS measurement (Analytik Jena Spekol 2000) parameters: reference—dH_2O; range 320–800 nm with 2 nm steps; light path 1 cm.

Determination of Molar Extinction Coefficients: The molar extinction coefficient (ε) of HABSA, HABSA-Ac and *p*-NP in 1% DMSO was measured at pH 8.5 and additionally in 100% DMSO for HABSA. The stock solution of 0.5 mM HABSA was prepared by dissolving 15.9 mg of dye in 15 mL of DMSO, then diluting it with DMSO and 10 mM Tris–HCl, pH 8.5, buffer to 38.13 µM (1% or 100% DMSO). The stock solution of 50 mM HABSA-Ac was prepared by dissolving 160 mg of substrate in 10 mL of DMSO, then diluting to 0.5 mM (1% DMSO) with buffer. For *p*-NP, a 1 mM stock solution was prepared by dissolving 0.139 g of *p*-NP in 10 mL of DMSO and diluting to 10 µM (1% DMSO) with DMSO and buffer. Absorbance values were measured in triplicate at a 320–800 nm range, with a light path of 1 cm. For reference measurements, 1% DMSO in a 10 mM pH 8.5 buffer solution was used. The molar extinction coefficients were calculated using the Beer–Lambert law.

Stability of HABSA-Ac in DMSO: The stability of HABSA-Ac in DMSO was evaluated by UV–vis spectroscopy. A 20 mM HABSA-Ac solution was prepared by dissolving 0.128 g of the substrate in 20 mL of DMSO and diluting to a final concentration of 0.2 mM. 2 mL of this solution was stored at −20°C, 4°C, 20°C, 40°C, 60°C and 80°C. UV–vis spectra of each solution were recorded every 24 h for 7 days. Spectroscopy parameters: reference—DMSO; range: 320–800 nm with 1 nm steps; quartz cuvette with 0.5 cm light path.

2.4 | Esterase Activity Assay With *p*-NP Acetate as a Substrate

The initial 20 mM *p*-NPA substrate solution was prepared by dissolving 36.2 mg of *p*-NPA in 10 mL of DMSO. Initial 2.67 mL of 168 mM Tris–HCl (pH 8.5) buffer and 0.03 mL of substrate were combined in the cuvette, which was placed within a 1.0 cm light path. The reaction was initiated by adding 0.3 mL of enzyme solution. Substrate autohydrolysis control measurements were conducted by substituting the enzyme with water. Final concentrations in the cuvette (reaction) were as follows: 0.2 mM *p*-NPA, 10% enzyme solution (v/v), 1% DMSO, 150 mM Tris–HCl. The kinetic spectroscopy measurements were performed at 400 nm for 180 s with a data recording rate of 2 s. 1 activity unit (1 U) is defined as the formation of 1 µmol of *p*-NP per 1 min at pH 8.5 and 20°C.

$$\upsilon = \frac{Slope_E - Slope_O}{\varepsilon_{400} \times l} \times 60$$

where υ—catalysis rate (μM^{-1} min^{-1}); $Slope_E$—absorption slope in enzymatic reaction (AU s^{-1}); $Slope_o$—absorption slope in autohydrolysis reaction (AU s^{-1}); ε_{400}—*p*-NP molar extinction coefficient (0.0191 μM^{-1} cm^{-1}); *l*—cuvette light path (1.0 cm); 60—factor to convert seconds to minutes.

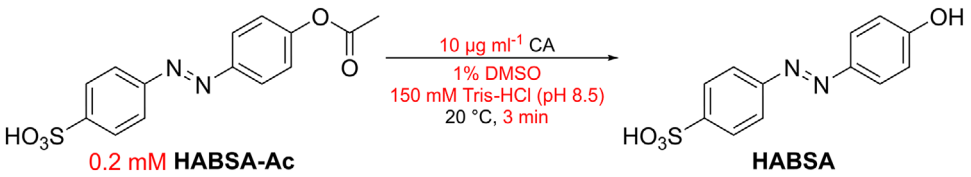

SCHEME 2 | The HABSA-Ac assay reaction catalysed by carbonic anhydrases. Varied and optimised conditions are highlighted in red.

2.5 | Esterase Activity Assay With Indoxyl Acetate as a Substrate

The assay was adapted from a method published by Baliukynas et al. [26]. In brief, the reaction constituents were increased 10-fold, and measurements were performed in a 1 cm light path cuvette. A buffer solution (2.4 mL) containing 17.5 mM HEPES and 17.5 mM imidazole at pH 7.2 was mixed with 0.3 mL of substrate in the cuvette. The reaction's initiation was marked by adding 0.3 mL of an enzyme solution, including control measurements for substrate autohydrolysis, in which the enzyme was replaced with buffer. The kinetic spectroscopic parameters were set as follows: the reference was a 1% EtOH buffer solution; the measurement delay was 5 s; the wavelength was 375 nm; the duration was 600 s; and the data recording rate was 5 s. One activity unit (1 U) is defined as the formation of 1 µmol of indoxyl per 1 min at pH 7.2 and 20°C.

$$v = \frac{Slope_E - Slope_O}{\varepsilon_{375} \times l} \times 60$$

where v—reaction rate (μM^{-1} min^{-1}); $Slope_E$—absorption slope in enzymatic reaction (AU s^{-1}); $Slope_o$—absorption slope in autohydrolysis reaction (AU s^{-1}); ε_{375}—indoxyl molar extinction coefficient (0.00254 μM^{-1} cm^{-1}) [27]; l—cuvette light path (1.0 cm); 60—factor to convert seconds to minutes.

2.6 | Development of an Enzymatic Activity Assay With HABSA-Ac as a Substrate

Approximately 1.602 mL of buffer and 0.018 mL of substrate were combined in a 0.5 cm cuvette. The enzymatic reaction and kinetic measurements were initiated by adding 0.18 mL of enzyme (bCAII) solution (Scheme 2). For the substrate autohydrolysis control measurements, the enzyme was substituted with the appropriate buffer. The kinetic spectroscopy parameters were as follows: reference—1% DMSO solution in the corresponding buffer; measurement delay—5 s; wavelength—428 nm; data recording rate—2 s. The calculation of bCAII catalytic rates is performed using the formula below. One activity unit (1 U) is defined as the formation of 1 µmol of HABSA per 1 min at pH 8.5 and 20°C.

$$v = \frac{Slope_E - Slope_O}{\varepsilon_{428} \times l} \times 60$$

where v—reaction rate (μM^{-1} min^{-1}); $Slope_E$—absorption slope in enzymatic reaction (AU s^{-1}); $Slope_o$—absorption slope in autohydrolysis reaction (AU s^{-1}); ε_{428}—HABSA molar extinction coefficient (0.0175 μM^{-1} cm^{-1}) l—cuvette light path (0.5 cm); 60—factor to convert seconds to minutes.

The optimal final substrate concentration was determined using HABSA-Ac solutions ranging from 0.1 to 1.0 mM, prepared in 1% DMSO and 10 mM Tris–HCl (pH 8.5), in the absence of enzyme. To identify the most suitable buffer type, reactions were conducted in 10 mM buffers at pH 8.5, including Tris–HCl, 2-amino-2-methyl-1,3-propanediol (AMPD), sodium borate ($NaBO_3$) and diethanolamine ($NH(EtOH)_2$), in the presence of 10 µg mL^{-1} of bovine carbonic anhydrase (bCAII). The optimal Tris–HCl buffer concentration was determined by performing assays at final concentrations of 10, 50, 100, 150 and 200 mM in a cuvette. The appropriate reaction duration was determined by measuring activity at 1, 3, 5, 10 and 20 min. To determine the optimal enzyme concentration for kinetic analysis as well as the assay's limit of detection and quantification, catalytic rates were measured using final bCAII concentrations of 0.1, 1 and 10 µg mL^{-1} in 150 mM Tris–HCl buffer.

The inhibition of bCAII was investigated using 34.4 µM (0.1 mg mL^{-1}) bCAII solutions incubated for 20 min either with potassium cyanide (KCN) or acetazolamide. Inhibitor concentrations were prepared at varying molar ratios relative to the enzyme: 1:1, 1:5, 1:20, 1:100 for KCN; and 1:0.25, 1:0.5, 1:1 for acetazolamide.

The influence of temperature on the rates of substrate autohydrolysis and catalysis was investigated in the 30°C–75°C range. The cuvette and buffer were equilibrated at the set temperature for 2 min, followed by the quick addition of substrate and enzyme or dH_2O. Temperature control was ensured using a water-jacketed cuvette holder connected to an external water-circulating thermostat.

2.7 | Lineweaver–Burk, Eisenthal–Cornish–Bowden, Arrhenius and Transition State Theory Plot Analysis

For each series of Michaelis–Menten kinetics measurements, the values of K_M and V_{max} were calculated from the Lineweaver–Burk (L–B) and Eisenthal–Cornish–Bowden (E–C–B) linear plots. Subsequently, the catalytic constants k_{cat} and k_{cat}/K_M were determined.

Observed activation energy ($E_{a,obs}$) and Arrhenius factor (A) were estimated from the Arrhenius plots, while observed enthalpy ($\Delta H^{\ddagger}_{obs}$) and entropy ($\Delta S^{\ddagger}_{obs}$) were estimated from the transition state theory (TST) linear plots. Equations for k_{cat}/K_M and observed transition state Gibbs energy ($\Delta G^{\ddagger}_{obs}$) calculations from thermodynamic data are available in the Supporting Information. The L–B, Arrhenius and TST plotting data for the linear functions ($y = ax + b$) are provided in Table 1.

TABLE 1 | Variables for L–B, Arrhenius and TST plots, with directly derived parameters from the respective plots.

Plot	*y* variable	*x* variable	Derivative parameters
L–B	$1/v$	$1/[S]$	$a/b = K_M$ $1/b = V_{max}$
Arrhenius	$\ln(v)$	$1/T$	$a = -E_{a,obs} / R$ $b = \ln A + \ln([S]_0[E]_0)$
TST[a,b]	$\ln(k_{eff}/T)$	$1/T$	$a = -\Delta H^{\ddagger}_{obs}/R$ $b = \ln(k_B/h) + (\Delta S^{\ddagger}_{obs} / R)$

[a] k_{eff}—Effective reaction rate (v) / $[S]_0$ for substrate autohydrolysis reactions or (v) / ($[E]_0[S]_0$) for enzymatic catalysis.

[b] R—Universal gas constant (8.3145 J mol^{-1} K^{-1}); k_B—Boltzmann constant (1.38 × 10^{-23} J K^{-1}); h—Plank constant (6.63 × 10^{-34} J s).

The E–C–B method utilised data consisting of initial catalysis rates (v) and corresponding substrate concentrations ($[S]$), which were used in linear function form $y(x) = ax + b$. The general function:

$$y(x)_{[S]} = \frac{v_{[S]}}{[S]}x + v_{[S]}$$

where $y(x)_{[S]}$—linear function for appropriate substrate concentration; $v_{[S]}$—initial catalysis rate for appropriate substrate concentration (μM^{-1} min^{-1}); $[S]$—substrate concentration (mM).

To calculate and tabulate the x-coordinates of intersection points, indicating K_M, between two functions, a generalised formula was used:

$$x\left([S]_i;[S]_j\right) = \frac{v_j - v_i}{\left(\frac{v_i}{[S]_i} - \frac{v_j}{[S]_j}\right)}$$

where $x([S]_i;[S]_j)$—x coordinate at the intersection between functions for a pair of $[S]_i$ and $[S]_j$ ($[S]_i \neq [S]_j$); v—initial catalysis rate for appropriate substrate concentration (μmol L^{-1} min^{-1}); $[S]$—substrate concentration (mM).

Note that functions for the same $[S]$ functions were parallel and do not intersect. In addition, the array was symmetric, meaning that $x([S]_i;[S]_j)$ yielded the same result as $x([S]_j;[S]_i)$; therefore, duplicate results were not included. Any negative intersection values were removed from the array, as negative values are false. Maximum catalysis rate V_{max} was calculated using the x values from the arrays in the relevant $y(x)_{[S]}$ equations. The median K_M and V_{max} were determined, followed by the calculation of turnover number (k_{cat}) and specificity constant (k_{cat}/K_M):

$$k_{cat} = \frac{V_{max}}{[E] \times 60} \qquad k_{cat}/K_M = \frac{k_{cat}}{K_M \times 1000}$$

where k_{cat}—enzyme turnover number (s^{-1}); V_{max}—maximum catalysis rate (μM^{-1} min^{-1}); $[E]$—bCAII concentration in the reaction (0.344 μM); 60—minutes to seconds conversion factor; k_{cat}/K_M—substrate specificity constant (M^{-1} s^{-1}); K_M—Michaelis constant (mM); 1000—mM to M conversion factor.

2.7.1 | Standard Error Calculation

Standard errors for reaction rates, K_M, V_{max}, K_i, K_i', $E_{a,obs}$, $\Delta H^{\ddagger}_{obs}$ and $\Delta S^{\ddagger}_{obs}$ as well as the derived k_{cat}, k_{cat}/K_M, $\Delta H^{\ddagger}_{obs}$ and $\Delta G^{\ddagger}_{obs}$ were calculated using standard methods for sample standard deviation and error estimation:

$$s = \sqrt{\frac{\sum (x_i - \bar{x})^2}{n - 1}} \qquad SE = \frac{s}{\sqrt{n}}$$

where s—sample standard deviation; x_i—sample value; $\bar{x}$—sample mean; n—number of samples; SE—standard error.

2.8 | Bradford Protein Assay

Bradford reagent was prepared according to the original method protocol [28]. The calibration curve was produced using a standard solution of 0.5 mg mL^{-1} BSA at a final concentration of 1.5–15.0 μg mL^{-1}, and measuring the absorbance. Protein sample measurements used 10–100 μL of sample diluted with 0.15 M NaCl to a final volume of 0.3 mL. Then, 3 mL of Bradford reagent was added, mixed and incubated for 2.0 min at 20°C. After incubation, the absorbance at 595 nm was measured. The reference measurement used 0.3 mL of 0.15 M NaCl, and the protein sample was omitted. Protein concentration was calculated using the formula below:

$$C_E = \frac{A_{595}}{Slope} \times \frac{V_R}{V_E}$$

where C_E—protein concentration in the initial sample (mg mL^{-1}); A_{595}—absorption at 595 nm; Slope—calibration curve slope; V_R—total reaction volume (3.3 mL); V_E—protein solution volume (mL).

3 | Results and Discussion

The research focus in this study was to use azo coupling between phenol and acidic aniline derivatives to produce several dyes (Scheme 3).

Phenyl azo dyes contain a phenol group linked to an aromatic system via an azo bridge, exhibiting strong light absorption due to n → π^* and π → π^* transitions. These compounds also exhibit relatively high redox potential and low susceptibility to nucleophilic or electrophilic reactions [29]. It ensures their structural stability and consistent spectral properties across a variety of conditions [30]. The wide selection of phenol and aniline derivatives allows for fine-tuning of properties needed for dye application in different scenarios [25]. Deprotonation of the phenol group shifts absorption from the near-UV to the visible range, making them useful and attractive for UV–vis assays. A key example is *p*-NP esters, which form *p*-nitrophenoxide in enzyme assays for esterases, lipases and phosphatases [31–33]. Another concern is substrate solubility, which is crucial, as enzymatic assays use aqueous buffers. Robust enzymes, such as lipases, can easily tolerate the presence of organic solvents. However, it is

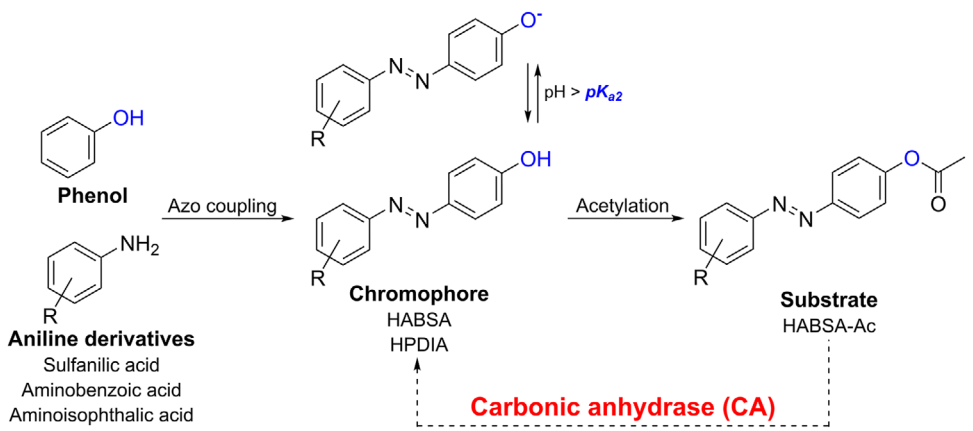

SCHEME 3 | Generalised approach for substrate synthesis and application.

known that some organic solvents, even at low concentrations of 1%–2%, can reduce CA activity [34, 35]. Thus, the variant with the highest water solubility was selected for acetylation to produce the substrate, determination of pK_{a2} and spectroscopic properties. Substrate catalysis conditions were optimised by measuring catalytic rates of a well-characterised CA used as a reference model. Optimisation included buffer type and concentration, as well as substrate and enzyme concentrations, and the duration of the assay. The validation of the assay was performed by determining Michaelis–Menten kinetic parameters, substrate performance at elevated temperatures and exploring enzyme inhibition. Seven other hydrolases were tested with the designed assay and compared with the results of *p*-NPA and indoxyl acetate assays.

3.1 | The Synthesis and Characterisation of Dyes and Substrate 4-(4-Acetoxyphenylazo) Benzenesulfonic Acid

Initially, for the synthesis of an azo dye, three compounds were considered. 4-(4-Hydroxyphenylazo)benzoic acid was not produced due to its reported limited solubility in water [30]. The other two considered dyes, 4-(4-hydroxyphenylazo)benzenesulfonic acid (HABSA) and 5-(4-hydroxyphenylazo)isophthalic acid (HPDIA), were successfully synthesised. For HABSA, minor adjustments in reagent ratios and recrystallisation solvent resulted in a yield increase of 4%, achieving a total yield of 76%. The synthesis of HPDIA was developed by replacing the initial aromatic amine in the HABSA method with 5-aminoisophthalic acid and altering the recrystallisation solvent, yielding 61%. NMR confirmed the structure and purity of both products. Initial testing revealed that HPDIA has limited solubility in water (0.036 mg mL^{-1}; 0.125 mM), while HABSA exhibited a solubility of 2.2 mg mL^{-1} (7.9 mM). Due to the anticipated further decrease in solubility upon acetylation, HPDIA was excluded from further study.

The chosen dye, HABSA, was used to synthesise the substrate 4-(4-acetoxyphenylazo)benzenesulfonic acid (HABSA-Ac). Dissolution in DMF followed by heating with acetic anhydride under modified conditions (temperature raised from 70°C to 75°C, reaction time extended from 'overnight' to 20 h, and additional washing steps) produced a high-quality product as confirmed by NMR. The yield reached up to 70%, with an overall production yield of 53%. The solubility of the compound was determined to be around 0.42 mg mL^{-1} (1.3 mM).

To be considered suitable for application, dyes and substrates used in spectrophotometric activity assays must possess several key characteristics. Notably, the compounds must exhibit a high molar absorption coefficient (ε), which is influenced by the functional groups conjugated to the aromatic system. For this reason, phenol-based azo dyes were selected for this study. When their hydroxyl group is deprotonated, these compounds undergo a bathochromic shift (red shift). Consequently, the initially examined feature was the pK_a of the phenolic group (pK_{a2}), which indicates the pH at which half of the phenolic —OH groups are deprotonated. Potentiometric titration of HABSA solution with 0.1 M KOH revealed an equivalence point at pH 8.32, corresponding to the deprotonation of phenolic —OH group (Figure S1). UV–vis spectroscopy confirmed this result: below pH 8.0, an absorption maximum at 350 nm was observed, while above pH 8.0 two overlapping maxima appeared at 374 nm and 420–440 nm. At pH 8.5, only the 420–440 nm maximum remained, confirming phenolic deprotonation and a bathochromic shift (Figure S2). The observed shift from near-UV to visible light (428 nm) above pH 8.0 ensures suitability for spectrophotometric assays, as absorbance in the visible range minimises interference from protein or nucleic acid background. Wide spectral measurements (320–800 nm) of 5 μM dye solutions in 1% DMSO, 10 mM Tris–HCl (pH 8.5) showed that HABSA had an absorption maximum at 428 nm with a molar extinction coefficient (ε) of 0.0175 μM^{-1} cm^{-1}. For comparison, *p*-NP, a widely used substrate component, exhibited ε_{400} = 0.0191 μM^{-1} cm^{-1} under the same conditions. As the molar extinction coefficient directly correlates with UV–vis spectroscopy analytical signal intensity, higher values allow for better signal resolution from the baseline, greater sensitivity to minor changes in substrate concentration and lower limit of detection. The obtained value for HABSA would be classified as very (> 0.01 μM^{-1} cm^{-1}), which is typical for dye compounds and similar to *p*-NP, suggesting that it can provide sensitive detection in enzyme assays. Furthermore, the longer absorption wavelength minimises potential interference from near-UV-absorbing compounds abundant in protein extracts or cultivation media. HABSA-Ac also absorbed at 428 nm but with

a substantially lower ε of 0.0013 μM^{-1} cm^{-1}, measured after a short delay due to immediate autohydrolysis. It shows an intrinsic absorption spectrum overlapping at ε_{428} with HABSA, though with an over 10-fold decrease.

The last investigated characteristic was the stability of HABSA-Ac. During the course of the determination of its molar extinction coefficient, autohydrolysis was observed within minutes in an aqueous solution. UV–vis monitoring of HABSA-Ac in DMSO solutions stored at −20°C, 4°C, 20°C, 40°C, 60°C and 80°C showed negligible spectral changes (< 0.05 AU) below 80°C after 72 h. After 7 days, differences reached 0.1 AU, indicating noticeable degradation. At 80°C, substrate quality decreased after 24 h. These observations suggested that the storage solvent, rather than temperature, was the primary driving force behind substrate degradation. Taken together, HABSA proved to be a soluble, spectrally suitable and stable dye, whereas its acetylated derivative, HABSA-Ac, despite successful synthesis, exhibited instability in aqueous environments, limiting its long-term use.

3.2 | Development of a CA Activity Assay Using HABSA-Ac as Substrate

An analysis of the substrate and dye spectral properties indicated that a pH of 8.5 was the minimum required for the HABSA-Ac spectrophotometric assay. This pH is suitable, as it falls within the typical operational range of CAs [36], is used in CO_2 hydration-based activity assays [37] and alkaline chemo-enzymatic CO_2 capture systems [38], supporting the assay's applicability to enzyme activity studies. Importantly, this pH ensured complete deprotonation of the phenolic group in HABSA, resulting in the bathochromic shift necessary for high sensitivity. Since HABSA and HABSA-Ac share the same absorption maximum at 428 nm, the substrate concentration was limited by the overlap of the substrate and product signals. Too high a concentration increases initial absorption, risking exceeding the linear detection range of spectrophotometry [39], while too low a concentration reduces assay sensitivity. The optimal substrate concentration was determined to ensure steady-state kinetics while maintaining assay sensitivity. Based on extinction coefficients, a 0.2 mM HABSA-Ac solution was expected to yield ∼0.1 absorbance units (AU) in a 1 cm cuvette. Experimental data confirmed absorption values of 0.136 AU (0.2 mM) and 0.080 AU (0.1 mM). Therefore, 0.2 mM was selected as the optimal substrate concentration, providing a reliable signal intensity without saturating the detector.

A commercially available α-family carbonic anhydrase II (bCAII) from bovine erythrocytes was selected as the enzyme for assay development. Its biochemical properties are well investigated [40], making it a perfect model protein for substrate assessment, validation and comparison. The fluorescent thermal shift assay showed that HABSA and HABSA-Ac do not inhibit this enzyme within the pH 7.0–8.5 range. ATR-FTIR analysis confirmed the enzymatic hydrolysis product as the HABSA. To evaluate buffer suitability, catalytic reactions were performed in four buffers at 10 mM: Tris–HCl, AMPD, $NaBO_3$ and $NH(EtOH)_2$. The catalysis rates (μM min^{-1} at 428 nm) indicated that $NH(EtOH)_2$ reduced activity, while Tris–HCl, AMPD and $NaBO_3$ yielded consistent results (Figure 1A).

Although borate is known to inhibit certain CA isoforms [41], bCAII was unaffected under the tested conditions, indicating enzyme-specific effects. Tris–HCl was ultimately selected due to its established role in CA studies [42]. Buffer concentration effects were then examined between 10 and 200 mM. Reaction rates gradually increased with concentration and peaked at 150 mM, beyond which activity declined (Figure 1B). This finding highlights the role of ionic strength in enzyme catalysis: insufficient ionic strength reduces activity, while excessively high concentrations hinder catalysis, likely due to perturbations in protein–solvent interactions.

An important consideration in assay development is the measurement time. Spectrophotometric measurements require a duration of between 1 min and several hours to yield reliable results, depending on the enzyme's catalysis rate and the assay's sensitivity [26, 37]. The effect of measurement duration was assessed over reaction times of 1, 3, 5, 10 and 20 min. A burst phase during the first 20–30 s limited the linearity of 1-min measurements, while extending beyond 3 min provided no additional benefit. Three minutes was identified as the optimal duration.

Activity assays are typically designed to yield reliable results while minimising enzyme use. One method to determine the appropriate enzyme concentration is to perform reactions with progressively lower enzyme amounts. As enzyme concentration decreases, reaction rates decrease linearly until they deviate at the assay's limit of quantification. The lowest distinguishable reaction rate above the baseline (autohydrolysis) defines the limit of detection. The last factor in assay development was the identification of the optimal enzyme concentration and the establishment of the limits of quantification and detection. Enzyme concentration limits were determined by testing bCAII in the range of 10–0.1 μg mL^{-1}. At 1 μg mL^{-1} (34.4 nM), errors in catalysis rates exceeded ± 2.0%, defining the assay's limit of quantification. At 0.1 μg mL^{-1} (3.44 nM), the minimal measurable rate difference compared with autohydrolysis (0.0006 AU min^{-1}) was established as the limit of detection. For practical use, 10 μg mL^{-1} bCAII was chosen to ensure robust activity measurements. In summary, the optimised assay conditions were 150 mM Tris–HCl (pH 8.5), 0.2 mM HABSA-Ac, 1% DMSO and 10 μg mL^{-1} bCAII, with a reaction time of 3 min at 20°C. One unit (1 U) of enzyme activity was defined as the formation of 1 μmol HABSA per minute under these conditions.

3.3 | Validation of the Developed CA Activity Assay Using HABSA-Ac as a Substrate

Following the establishment of the HABSA-Ac assay conditions, validation was performed through kinetic analysis. The kinetic parameters Michaelis constant (K_M), maximum catalytic rate (V_{max}), enzyme turnover number (k_{cat}) and specificity constant (k_{cat}/K_M) were determined for bCAII. Catalysis rates were measured across a substrate concentration range of 0.1–1.0 mM in independent triplicate, within an absorption window of 0.1–1.0 AU. Higher substrate concentration could not be employed due to the substrates' intrinsic absorption maximum at 428 nm exceeding 1.0 AU. Within this concentration range, reaction rates

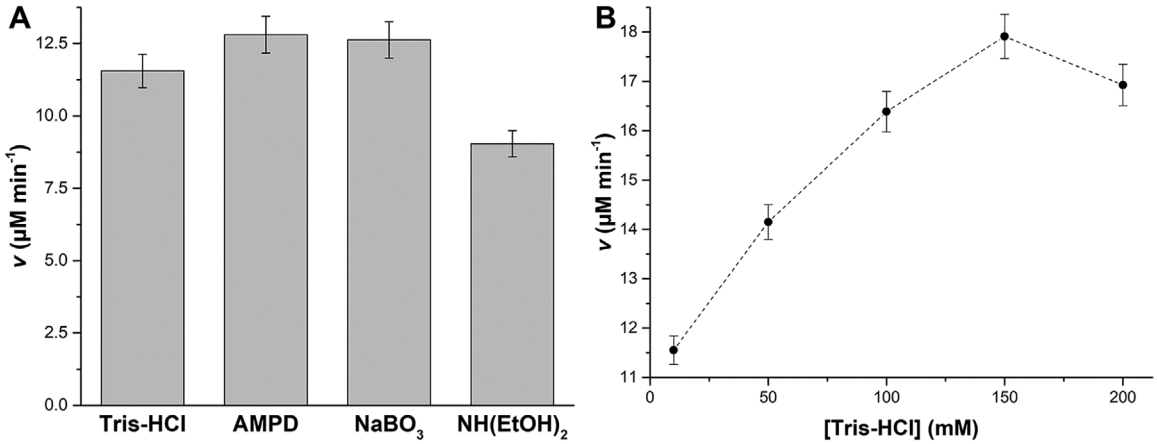

FIGURE 1 | Catalysis rates of bCAII in different buffer conditions: (A)—Effect of selected buffers (10 mM); (B)—Influence of the Tris–HCl buffer concentration (10–200 mM). Reaction conditions: pH 8.5, 20°C, 0.2 mM HABSA-Ac, 10 μg mL^{-1} bCAII.

TABLE 2 | Initial kinetic parameters for HABSA-Ac catalysis by bCAII, estimated using Lineweaver–Burk (L–B) and Eisenthal–Cornish–Bowden (E–C–B) methods.

Kinetic parameter	L–B	E–C–B
K_M (mM)	9.1 ± 1.1	9.5 ± 1.8
V_{max} (μM^{-1} min^{-1})	312 ± 34	334 ± 62
k_{cat} (s^{-1})	15.1 ± 1.7	16.2 ± 3.0
k_{cat} / K_M (M^{-1} s^{-1})[a]	1674 ± 33	1697 ± 24

[a]Values were calculated using individual measurement k_{cat}/K_M data.

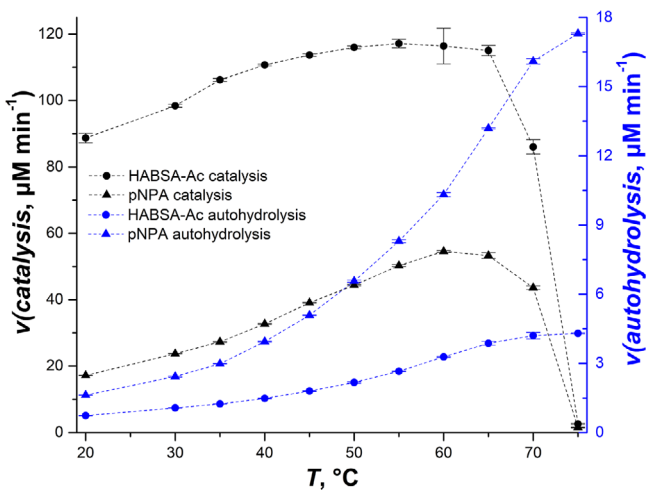

FIGURE 2 | HABSA-Ac and *p*-NPA autohydrolysis and catalysis rate dependency on the temperature (150 mM Tris–HCl pH 8.5, 10 μg mL^{-1} bCAII).

increased linearly and did not reach enzyme saturation (Figure S3), indicating that the tested substrate concentrations remained below K_M and that the reaction rates were significantly lower than V_{max}. The kinetic parameters were estimated using the commonly applied Michaelis-Menten linearization methods: the L–B and E–C–B methods. Table 2 summarises the results.

The analysis showed that the average K_M value was approximately 9.3 mM, revealing that the highest substrate concentration tested (1 mM) was more than nine times lower than the established K_M values. Asadi et al. [43] reported K_M values of 8.9 mM for bCAII with *p*-NPA as the substrate, indicating comparable recognition by the enzyme. However, the catalytic efficiency (k_{cat}/K_M) of *p*-NPA was around 400 M^{-1} s^{-1}, suggesting that HABSA-Ac was a more efficient substrate for bCAII by around four-fold under similar conditions. Ultimately, HABSA-Ac catalytic parameters were broadly consistent across replicate measurements, although the large spread underscores the inherent difficulty of measuring kinetic constants when substrate concentrations are substantially below the K_M. For future research, several technical changes could be implemented to improve reaction rate observations: (i) use a cuvette with a shorter light path (< 0.5 cm) would allow the use of higher initial substrate concentrations without exceeding 1.0 AU absorption threshold; or (ii) employment of a specialised UV–vis spectrophotometer designed to accurately measure absorption values and temporal changes above 1.0 AU. There is also the possibility of chemically modifying the substrate molecule by introducing new functional groups to improve its physical and chemical properties. This would require a ground-up reevaluation of the new dye and substrate properties, and optimisation of assay conditions.

One drawback of *p*-NPA as a substrate is its poor thermal stability. Characterisation of thermo- or hyperthermostable CAs can involve conducting assays at temperatures approaching the boiling point of aqueous media [44]. Under these conditions, substrate autohydrolysis rates can approach the catalytic rates of enzymes with low esterase activity, thereby reducing measurement resolution, even when side reactions are accounted for. Therefore, the autohydrolysis and catalytic rates of HABSA-Ac were investigated in a temperature range of 30°C–75°C using established buffer, substrate and enzyme concentrations. Temperature equilibration was ensured before and during measurements using a water-jacketed cuvette holder connected to an external water-circulating thermostat. For comparison, measurements with *p*-NPA were performed in parallel using 0.2 mM substrate in 150 mM Tris–HCl (pH 8.5) buffer. All measurements were performed in triplicate. (Independent) The reaction rate dependents on temperature are summarised in Figure 2.

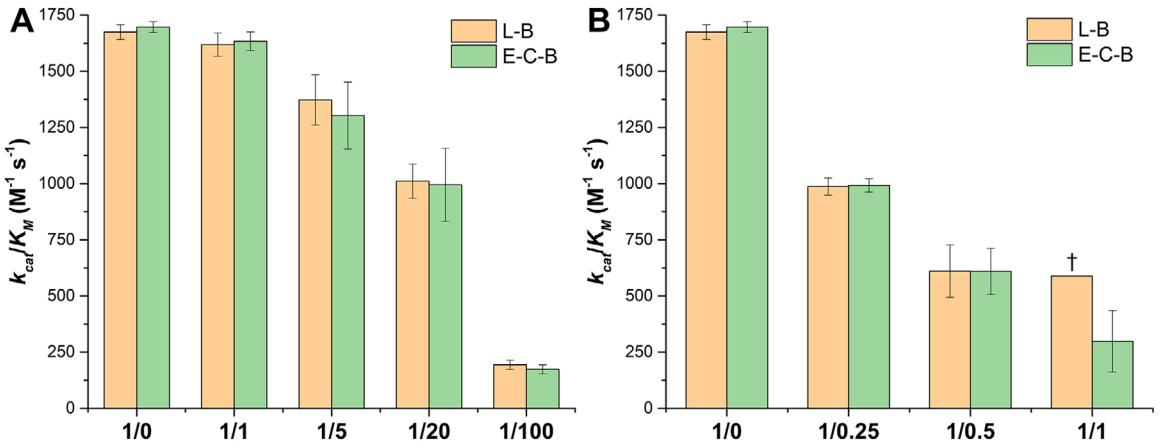

FIGURE 3 | Results of k_{cat}/K_M with various [bCAII]/[Inhibitor] molar ratios, calculated using L–B and E–C–B: (A)—Inhibition by KCN; (B)—Inhibition by acetazolamide. † denotes analysis with negative results. Reaction conditions: 150 mM Tirs-HCl pH 8.5, 20°C, 0.2 mM HABSA-Ac, 10 μg mL^{-1} bCAII.

The data showed that catalytic rates steadily increased and peaked at 60°C, then decreased and completely lost activity at 75°C. These findings align with the melting temperature of bCAII, which is reported to be 68.8°C at similar conditions [45]. The increase in catalytic rate per temperature was comparable for both substrates, while substrate autohydrolysis rates exhibited significantly different profiles. For HABSA-Ac, from 20°C to 75°C, the decomposition rate increased by approximately 3.6 μM min^{-1} in total. Meanwhile, *p*-NPA surged more than 10-fold, from 1.6 to 17.3 μM min^{-1}, highlighting its sensitivity to environmental conditions. The thermostability of HABSA-Ac is advantageous, as autohydrolysis often complicates CA kinetic measurements, particularly at alkaline pH or elevated temperatures. For example, Fredslund et al. [46] reported that thermostable alkaline CA with low esterase activity could not be reliably assayed with *p*-NPA above pH 7.5 due to excessive autohydrolysis [46].

The collected catalysis reaction data, in the range of 30°C–55°C, were utilised in Arrhenius and TST plotting and analysis. Since the HABSA-Ac and *p*-NPA assays used a substrate concentration of 0.2 mM—significantly below the established K_M—the Arrhenius and TST analyses yielded the k_{cat}/K_M parameter. Analysis of autohydrolysis reactions utilised data from 20°C to 75°C. Constructed plots are available in Figures S4–S7, while derived k_{cat}/K_M, $E_{a,obs}$, $\Delta H^{\ddagger}_{obs}$, $\Delta S^{\ddagger}_{obs}$ and $\Delta G^{\ddagger}_{obs}$ are summarised in Tables S1 and S2. In short, the computed k_{cat}/K_M of HABSA-Ac catalysis were as follows: 2251 ± 796 M^{-1} s^{-1} in Arrhenius analysis and 2249 ± 26 M^{-1} s^{-1} in TST. Compared to the results obtained using the Michaelis–Menten kinetic model (1674 ± 33 M^{-1} s^{-1} and 1697 ± 24 M^{-1} s^{-1}), the values were noticeably higher but not unreasonable. These discrepancies could have arisen from limitations in HABSA-Ac concentration and from error propagation commonly recognised in linearised models [47]. The analysis of *p*-NPA catalysis produced k_{cat}/K_M of 409 ± 78 M^{-1} s^{-1} and 413 ± 4 M^{-1} s^{-1}, closely agreeing with published results [43]. The ratio of specificity constants indicated that HABSA-Ac was catalysed more effectively than *p*-NPA by over five-fold. Compared with published results on the hydrolysis of fluorogenic coumarin esters by bCAII [48], HABSA-Ac catalysis at 20°C was similar in rate, but its autohydrolysis was more than 100-fold higher, indicating further area for improvement.

In summary, this investigation confirmed that HABSA-Ac exhibited substrate properties comparable to, and in some respects superior to, the classical substrate *p*-NPA.

3.4 | Assessment of the CA Activity Assay for Monitoring the bCAII Inhibition Process

One way to evaluate the capabilities and limitations of an enzymatic assay is to assess its inhibition of the target enzyme, thereby highlighting its robustness and performance in low-activity scenarios. The bCAII is frequently used as a referenced CA in research involving mechanism studies or CAs applications in CO_2 sequestration [8]. Consequently, it has a wide selection of well-known and well-researched inhibitors, such as cyanides (CN^-), thiocyanates (SCN^-), azides (N_3^-) [49] or the commercially available sulfonamides [50]. The present study selected potassium cyanide (KCN) and 2-acetylamino-1,3,4-thiadiazole-5-sulfonamide (acetazolamide) based on their high affinity for bCAII [49]. Enzyme inhibition assays were performed by mixing bCAII with each inhibitor at defined molar ratios and measuring catalytic activity across varying substrate concentrations, as previously described. Substrate autohydrolysis rates were also assessed in the presence of an inhibitor; however, no significant differences were observed compared to control conditions. Kinetic parameters were calculated using the L–B and E–C–B methods from independent triplicate measurement data. The k_{cat}/K_M values for both inhibitors are presented in Figure 3, while the full set of kinetic parameters (K_M, V_{max}, k_{cat} and k_{cat}/K_M) is provided in Figure S8.

The analysis of k_{cat}/K_M revealed that bCAII inhibition by KCN began with a slight decrease at the 1:1 ratio and continued to increase with increasing inhibitor concentration. The same trend was observed in other kinetic parameters (K_M, V_{max} and k_{cat}). In contrast, acetazolamide reduced all kinetic parameters, except K_M, which remained relatively stable across varying inhibitor concentrations. It should be noted that catalytic rates at the ratio of 1:1 reached the assay's limit of quantification, resulting in two out of three measurements showing negative values (denoted with †).

TABLE 3 | The inhibition constants calculated using Dixon and C–B plots.

	Inhibitor	
	KCN	Acetazolamide
Dixon plot—K_i (μM)	3.00 ± 0.14	0.105 ± 0.002
E–C plot—K_i' (μM)	0.88 ± 1.12	0.104 ± 0.073

The observed decrease in both V_{max} and K_M with increasing KCN concentrations supported a mixed inhibition mechanism, whereas acetazolamide displayed non-competitive inhibition, reducing V_{max} without significantly altering K_M. To confirm inhibition mechanisms, Dixon and Cornish–Bowden (C–B) plots were constructed. The Dixon plot estimates K_i by plotting $1/v$ against $[I]$ at varying $[S]$, yielding $-K_i$ at the x-intercept [51]. The C–B plot, suited for mixed inhibition, plots $[S]/v$ versus $[I]$, where the x-intercept gives $-K_i'$ [52]. Data points at the highest inhibitor concentrations were excluded because reaction rates fell below the quantification limit. Inhibition constants were calculated following three steps: (i) tabulation of x-coordinate intercepts, (ii) exclusion of positive intersection values and (iii) calculation of the median value. Standard deviations and standard errors were then determined. The Dixon and C–B plots are provided in Figure S9, and inhibition constants are summarised in Table 3.

For KCN, the Dixon plot intersected below the x-axis, while the C–B plot intersected above it, consistent with mixed inhibition. Among the two, the Dixon plot yielded more accurate and consistent results. For KCN, the estimated K_i compared reasonably well with the previously reported value of 2.6 μM at pH 7.55 (Tris–HCl buffer) [15]. Although differences in assay conditions, particularly pH, limit the comparability of assays. For acetazolamide, both plots showed excellent agreement between K_i and K_i' values, in line with a non-competitive inhibition mechanism and literature values (~0.2 μM at pH 8.45 in 9 mM Tris–HCl with 10% [v/v] acetonitrile) [16]. These findings were consistent with the established inhibitory profiles of cyanides and sulfonamides against CAs [16, 50]. In short, this study demonstrated the robustness of the HABSA-Ac assay for analysing CA kinetics and inhibition mechanisms.

3.5 | Comparison of HABSA-Ac Performance With *p*-NPA and Indoxyl Acetate Activity Measurement Assays

To evaluate the selectivity of the HABSA-Ac assay, the hydrolysis of the substrate was tested with CAs, hydrolases and non-catalytic proteins. Five commercially available enzymes were used: carbonic anhydrase II (bCAII) from bovine erythrocytes—model CA with high esterase-like activity; a promiscuous recombinant esterase from *B. subtilis*; two highly active lipase preparations—Biorro LPS L and Novozymes Lipolase 100L; and a lysophospholipase product Finizym W as a reference for hydrolases with non-lipase activity. Several other CAs were also included: human carbonic anhydrase IX (hCAIX) known for its low esterase-like activity and two β-CAs from *P. aeruginosa* (psCA1 and psCA2) without esterase activity [53]. BSA was tested as a negative control. Protein concentrations for BSA, bCAII, esterase, hCAIX, psCA1 and psCA2 were standardised to 0.344 μM. The two lipase products were diluted due to their exceptionally high hydrolytic activity in the *p*-NPP assay. For benchmarking, two established esterase activity assays were used: the *p*-NPA assay (0.2 mM substrate in 150 mM Tris–HCl pH 8.5) and the indoxyl acetate (indoxyl-Ac) assay scaled from microplate to cuvette format—1 mM substrate in 14 mM HEPES-Imidazole pH 7.2 buffer [26]. Reaction rates for all enzymes across the three substrates are summarised in Table 4.

TABLE 4 | The reaction rates (μM^{-1} min^{-1}) obtained using HABSA-Ac, *p*-NPA and Indoxyl-Ac assays.

	Substrate		
	HABSA-Ac	*p*-NPA	Indoxyl-Ac
Autohydrolysis	0.76	1.67	0.37
BSA[a]	0.02	0.04	0.28
bCAII[a]	6.21	1.21	0.20
hCAIX[a]	1.38	0.67	1.65
psCA1[a]	0.05	0.27	0.37
psCA2[a]	0.06	0.33	0.33
Esterase[a]	35.32	41.19	298.57
LPS L[a]	2.20[b]	39.75	61.84
Lipolase 100L[a]	1.88[b]	6.29	221.45
Finizym W[a]	0.12[b]	0.83	0.83

[a]Results with substrate autohydrolysis rates subtracted.
[b]Protein concentrations in the assay were 10-fold higher than in *p*-NPA and indoxyl-Ac reactions.

The comparative analysis of the three substrates highlighted clear differences in selectivity and background stability. The results showed that autohydrolysis of HABSA-Ac was higher than that of indoxyl-Ac but lower than *p*-NPA. Meanwhile, HABSA-Ac demonstrated negligible (< 0.1 μM^{-1} min^{-1}) background reaction rates with BSA, psCA1 and psCA2, supporting the absence of non-specific catalysis and in line with reports that these *Pseudomonas* CAs are not typically associated with esterase activity [54]. Both psCAs hydrolysed *p*-NPA at measurable levels. A non-catalytic interaction was argued, as heat-deactivated (95°C, 5 min) psCA1 produced a reaction rate of 0.34 M^{-1} min^{-1} – slightly higher than that of non-heat-treated psCA1. Interestingly, indoxyl-Ac also produced measurable rates with BSA, psCA1 and psCA2, and displayed lower activity with bCAII than some non-catalytic proteins, further questioning its reliability as a selective CA substrate. The hCAIX showed low activity across the substrates, consistent with previous reports on its weak esterase-like catalytic properties [55]. The esterase from *B. subtilis* effectively hydrolysed all three substrates, as expected for a broad-specificity hydrolase, with particularly high rates toward indoxyl-Ac. In contrast, lipase and lysophospholipase catalysed hydrolysis of HABSA-Ac remained minimal even after protein concentrations were increased tenfold, whereas they exhibited strong activity on *p*-NPA and indoxyl-Ac. This poor substrate compatibility is a beneficial trait for HABSA-

Ac, as it reduces interference from lipases when applied to complex protein mixtures such as cell extracts or fermentation broths.

The assay sensitivities of HABSA-Ac, *p*-NPA and indoxyl-Ac were also compared based on the slopes (AU min^{-1}) calculated for hydrolysis catalysed by bCAII. The slope is suitable parameter to use because it directly shows the signal detected by the equipment and is not affected by data extrapolation or the kinetic model framework. In this analysis, the HABSA-Ac assay produced a slope of 0.109 ± 0.003 AU min^{-1}, *p*-NPA – 0.0231 ± 0.0001 AU min^{-1} and indoxyl-Ac – 0.0005 ± 0.0001 AU min^{-1}. It demonstrated that the HABSA-Ac hydrolysis produced a 4.7-fold higher signal than *p*-NPA and more than 200-fold higher than indoxyl-Ac.

In summary, HABSA-Ac exhibited moderate autohydrolysis, lower than that of *p*-NPA but higher than that of indoxyl-Ac, and showed enhanced selectivity for CAs relative to lipases and non-catalytic proteins. Although some cross-reactivity was observed in the esterase-mediated hydrolysis of HABSA-Ac, the assay nonetheless provided improved selectivity and sensitivity compared with both *p*-NPA and Indoxyl-Ac.

4 | Conclusions

This study reports the synthesis, characterisation and application of an acetylated phenyl azo dye (HABSA-Ac) as a novel substrate for assessing CA activity with esterase-like properties. The HABSA-Ac assay demonstrated several advantages over conventional substrates such as *p*-NPA and indoxyl acetate, including enhanced thermostability, improved selectivity toward CA isoforms and reduced susceptibility to lipase interference. Although further studies using a broader panel of CA isoforms are warranted to refine the assay, HABSA-Ac shows strong potential as a selective and practical tool for probing CA activity, with promising prospects for further optimisation and broader applicability in enzymatic assay development.

Author Contributions

Justinas Babinskas: data curation, formal analysis, investigation, methodology, validation, visualisation, writing – original draft. **Inga Matijošytė**: conceptualisation, funding acquisition, project administration, resources, supervision, writing – review and editing.

Acknowledgements

We especially thank members of the Department of Biothermodynamics and Drug Design (Life Sciences Center, Vilnius University), Dr. Lina Baranauskienė and PhD student Tautvydas Kojis for donating carbonic anhydrases and Dr. Aivaras Vaškevičius for performing NMR spectroscopy.

Funding

This project has received funding from the Research Council of Lithuania (LMTLT), agreement No. S-MIP-24-49.

Ethics Statement

The authors have nothing to report.

Conflicts of Interest

The authors declare no conflicts of interest.

Data Availability Statement

The authors declare that the data supporting the findings of this study are available within the paper and its Supporting Information files. Should any raw data files be needed in another format, they are available from the corresponding author upon reasonable request.

References

1. C. T. Supuran, "Carbonic Anhydrases: Novel Therapeutic Applications for Inhibitors and Activators," *Nature Reviews Drug Discovery* 7, no. 2 (2008): 168–181, https://doi.org/10.1038/nrd2467.

2. C. T. Supuran, "Structure and Function of Carbonic Anhydrases," *Biochemical Journal* 473, no. 14 (2016): 2023–2032, https://doi.org/10.1042/BCJ20160115.

3. E. L. Jensen, R. Clement, A. Kosta, S. C. Maberly, and B. Gontero, "A New Widespread Subclass of Carbonic Anhydrase in Marine Phytoplankton," *ISME Journal* 13, no. 8 (2019): 2094–2106, https://doi.org/10.1038/s41396-019-0426-8.

4. S. Lindskog, "Structure and Mechanism of Carbonic Anhydrase," *Pharmacology & Therapeutics* 74, no. 1 (1997): 1–20, https://doi.org/10.1016/S0163-7258(96)00198-2.

5. S. Lindskog and J. E. Coleman, "The Catalytic Mechanism of Carbonic Anhydrase," *PNAS* 70, no. 9 (1973): 2505–2508, https://doi.org/10.1073/pnas.70.9.2505.

6. B. H. Jo, J. H. Seo, and H. J. Cha, "Bacterial Extremo-α-Carbonic Anhydrases From Deep-Sea Hydrothermal Vents as Potential Biocatalysts for CO_2 Sequestration," *Journal of Molecular Catalysis B: Enzymatic* 109 (2014): 31–39, https://doi.org/10.1016/j.molcatb.2014.08.002.

7. A. Di Fiore, V. Alterio, S. Monti, G. De Simone, and K. D'Ambrosio, "Thermostable Carbonic Anhydrases in Biotechnological Applications," *International Journal of Molecular Sciences* 16, no. 7 (2015): 15456–15480, https://doi.org/10.3390/ijms160715456.

8. S. Talekar, B. H. Jo, J. S. Dordick, and J. Kim, "Carbonic Anhydrase for CO_2 Capture, Conversion and Utilization," *Current Opinion in Biotechnology* 74 (2022): 230–240, https://doi.org/10.1016/j.copbio.2021.12.003.

9. C. Molina-Fernández and P. Luis, "Immobilization of Carbonic Anhydrase for CO_2 Capture and Its Industrial Implementation: A Review," *Journal of CO2 Utilization* 47 (2021): 101475, https://doi.org/10.1016/j.jcou.2021.101475.

10. S. Peirce, M. E. Russo, R. Perfetto, et al., "Kinetic Characterization of Carbonic Anhydrase Immobilized on Magnetic Nanoparticles as Biocatalyst for CO_2 Capture," *Biochemical Engineering Journal* 138 (2018): 1–11, https://doi.org/10.1016/j.bej.2018.06.017.

11. I. M. Power, A. L. Harrison, and G. M. Dipple, "Accelerating Mineral Carbonation Using Carbonic Anhydrase," *Environmental Science & Technology* 50, no. 5 (2016): 2610–2618, https://doi.org/10.1021/acs.est.5b04779.

12. K. M. Wilbur and N. G. Anderson, "Electrometric and Colorimetric Determination of Carbonic Anhydrase," *Journal of Biological Chemistry* 176, no. 1 (1948): 147–154, https://doi.org/10.1016/S0021-9258(18)51011-5.

13. R. G. Khalifah, "The Carbon Dioxide Hydration Activity of Carbonic Anhydrase: I. Stop-Flow Kinetic Studies on the Native Human Isoenzymes B and C," *Journal of Biological Chemistry* 246, no. 8 (1971): 2561–2573, https://doi.org/10.1016/S0021-9258(18)62326-9.

14. C. T. Supuran, "Exploring the Multiple Binding Modes of Inhibitors to Carbonic Anhydrases for Novel Drug Discovery," *Expert Opinion on Drug Discovery* 15, no. 6 (2020): 671–686, https://doi.org/10.1080/17460441.2020.1743676.

15. Y. Pocker and J. T. Stone, "The Catalytic Versatility of Erythrocyte Carbonic Anhydrase. VI. Kinetic Studies of Noncompetitive Inhibition of Enzyme-Catalyzed Hydrolysis of *p*-Nitrophenyl Acetate," *Biochemistry* 7, no. 8 (1968): 2936–2945, https://doi.org/10.1021/bi00848a034.

16. Y. Pocker and J. T. Stone, "The Catalytic Versatility of Erythrocyte Carbonic Anhydrase. III. Kinetic Studies of the Enzyme-Catalyzed Hydrolysis of *p*-Nitrophenyl Acetate," *Biochemistry* 6, no. 3 (1967): 668–678, https://doi.org/10.1021/bi00855a005.

17. J. D. Cheeseman, A. D. Corbett, R. Shu, J. Croteau, J. L. Gleason, and R. J. Kazlauskas, "Amplification of Screening Sensitivity Through Selective Destruction: Theory and Screening of a Library of Carbonic Anhydrase Inhibitors," *Journal of the American Chemical Society* 124, no. 20 (2002): 5692–5701, https://doi.org/10.1021/ja017099.

18. J. A. Stewart and L. Ouellet, "The Trypsin Catalysed Hydrolysis of *p*-Nitrophenyl Acetate," *Canadian Journal of Chemistry* 37, no. 4 (1959): 751–759, https://doi.org/10.1139/v59-102.

19. B. Ali, S. Kaur, E. C. James, and S. S. Parmar, "Identification and Characterization of Hepatic Carboxylesterases Hydrolyzing Hydrocortisone Esters," *Biochemical Pharmacology* 34, no. 11 (1985): 1881–1886, https://doi.org/10.1016/0006-2952(85)90302-8.

20. D. M. Nedrud, H. Lin, G. Lopez, S. K. Padhi, G. A. Legatt, and R. J. Kazlauskas, "Uncovering Divergent Evolution of α/β-Hydrolases: A Surprising Residue Substitution Needed to Convert *Hevea brasiliensis* Hydroxynitrile Lyase Into an Esterase," *Chemical Science* 5, no. 11 (2014): 4265–4277, https://doi.org/10.1039/C4SC01544D.

21. M. Schmidt and U. T. Bornscheuer, "High-Throughput Assays for Lipases and Esterases," *Biomolecular Engineering* 22, no. 1 (2005): 51–56, https://doi.org/10.1016/j.bioeng.2004.09.004.

22. T. Fecker, P. Galaz-Davison, F. Engelberger, et al., "Active Site Flexibility as a Hallmark for Efficient PET Degradation by *I. sakaiensis* PETase," *Biophysical Journal* 114, no. 6 (2018): 1302–1312, https://doi.org/10.1016/j.bpj.2018.02.005.

23. V. Alterio, A. Di Fiore, K. D'Ambrosio, C. T. Supuran, and G. De Simone, "Multiple Binding Modes of Inhibitors to Carbonic Anhydrases: How to Design Specific Drugs Targeting 15 Different Isoforms?," *Chemical Reviews* 112, no. 8 (2012): 4421–4468, https://doi.org/10.1021/cr200176r.

24. Q. Tang, H. J. Quan, S. Liu, L. T. Liu, C. F. Chow, and C. B. Gong, "An Environmentally Friendly, Photocontrollable and Highly Recyclable Catalyst for Use in a One-Pot Three-Component Mannich Reaction," *Journal of Molecular Catalysis A: Chemical* 421 (2016): 37–44, https://doi.org/10.1016/j.molcata.2016.05.006.

25. D. Larsen, P. M. Bjerre, and S. R. Beeren, "Light-Controlled Out-of-Equilibrium Assembly of Cyclodextrins in an Enzyme-Mediated Dynamic System," *Chemical Communications* 55, no. 100 (2019): 15037–15040, https://doi.org/10.1039/C9CC08452E.

26. M. Baliukynas, A. Veteikytė, V. Kairys, and I. Matijošytė, "The Hydrolysis of Indoxyl Acetate: A Versatile Reaction to Assay Carbonic Anhydrase Activity by High-Throughput Screening," *Enzyme and Microbial Technology* 139 (2020): 109584, https://doi.org/10.1016/j.enzmictec.2020.109584.

27. M. Pohanka, M. Hrabinova, K. Kuca, and J. P. Simonato, "Assessment of Acetylcholinesterase Activity Using Indoxylacetate and Comparison With the Standard Ellman's Method," *International Journal of Molecular Sciences* 12, no. 4 (2011): 2631–2640, https://doi.org/10.3390/ijms12042631.

28. M. M. Bradford, "A Rapid and Sensitive Method for the Quantitation of Microgram Quantities of Protein Utilizing the Principle of Protein-Dye Binding," *Analytical Biochemistry* 72, no. 1 (1976): 248–254, https://doi.org/10.1016/0003-2697(76)90527-3.

29. S. Benkhaya, S. M'rabet, and A. El Harfi, "Classifications, Properties, Recent Synthesis and Applications of Azo Dyes," *Heliyon* 6, no. 1 (2020): e03271, https://doi.org/10.1016/j.heliyon.2020.e03271.

30. A. F. Danil de Namor, R. Traboulssi, and M. Salomon, "Solution Studies of Haptens Containing Azobenzoate and Substituted Azobenzoate Anions in Water and in Methanol," *Journal of the Chemical Society Faraday Transactions* 86, no. 3 (1990): 501, https://doi.org/10.1039/FT9908600501.

31. M. N. Levine, L. D. Lavis, and R. T. Raines, "Trimethyl Lock: A Stable Chromogenic Substrate for Esterases," *Molecules* 13, no. 2 (2008): 204–211, https://doi.org/10.3390/molecules13020204.

32. A. M. Gil-Rodríguez and T. P. Beresford, "Lipase Inhibitory Activity Assay for Fermented Milk," *MethodsX* 7 (2020): 100999, https://doi.org/10.1016/j.mex.2020.100999.

33. Z. Tang, H. Chen, H. He, and C. Ma, "Assays for Alkaline Phosphatase Activity: Progress and Prospects," *Trends in Analytical Chemistry* 113 (2019): 32–43, https://doi.org/10.1016/j.trac.2019.01.019.

34. R. Epton, M. E. Hobson, and G. Marr, "A Study of Carbonic Anhydrase Covalently Bound to a Poly(Acryloylmorpholine) Network in Aqueous/Organic Solvents," *Biochemical Society Transactions* 5, no. 1 (1977): 274–276, https://doi.org/10.1042/bst0050274.

35. R. Epton, M. E. Hobson, and G. Marr, "Synthesis and Properties of Expanded Poly(Acryloyl Morpholine)/Carbonic Anhydrase Conjugates With Catalytic Activity in Aqueous-Organic media," *Polymer* 18, no. 12 (1977): 1203–1207, https://doi.org/10.1016/0032-3861(77)90279-8.

36. V. M. Krishnamurthy, G. K. Kaufman, A. R. Urbach, et al., "Carbonic Anhydrase as a Model for Biophysical and Physical-Organic Studies of Proteins and Protein–Ligand Binding," *Chemical Reviews* 108, no. 3 (2008): 946–1051, https://doi.org/10.1021/cr050262p.

37. P. A. Fernández, M. Y. Roleda, R. Rautenberger, and C. L. Hurd, "Carbonic Anhydrase Activity in Seaweeds: Overview and Recommendations for Measuring Activity With an Electrometric Method, Using *Macrocystis pyrifera* as a Model Species," *Marine Biology* 165, no. 5 (2018): 88, https://doi.org/10.1007/s00227-018-3348-5.

38. T. Sharma, S. Sharma, H. Kamyab, and A. Kumar, "Energizing the CO_2 Utilization by Chemo-Enzymatic Approaches and Potentiality of Carbonic Anhydrases: A Review," *Journal of Cleaner Production* 247 (2020): 119138, https://doi.org/10.1016/j.jclepro.2019.119138.

39. H. Bisswanger, "Enzyme Assays," *Perspectives in Science* 1, no. 1 (2014): 41–55, https://doi.org/10.1016/j.pisc.2014.02.005.

40. D. T. Phan, R. C. Burns, G. Puxty, M. Williams, V. S. Haritos, and M. Maeder, "A Study of Bovine and Human Carbonic Anhydrases as a Model Enzyme System for CO_2 Hydration in Post Combustion Capture," *International Journal of Greenhouse Gas Control* 37 (2015): 85–89, https://doi.org/10.1016/j.ijggc.2015.03.016.

41. Z. S. Yusuf, T. K. Uysal, E. Simsek, et al., "The Inhibitory Effect of Boric Acid on Hypoxia-Regulated Tumour-Associated Carbonic Anhydrase IX," *Journal of Enzyme Inhibition and Medicinal Chemistry* 37, no. 1 (2022): 1340–1345, https://doi.org/10.1080/14756366.2022.2072837.

42. X. Li, R. Zhou, H. Yang, et al., "Properties of Carbonic Anhydrase-Containing Active Coatings for CO_2 Capture," *Processes* 12, no. 4 (2024): 810, https://doi.org/10.3390/pr12040810.

43. V. Asadi, R. Kardanpour, S. Tangestaninejad, M. Moghadam, V. Mirkhani, and I. Mohammadpoor-Baltork, "Novel Bovine Carbonic Anhydrase Encapsulated in a Metal–Organic Framework: A New Platform for Biomimetic Sequestration of CO_2," *RSC Advances* 9, no. 49 (2019): 28460–28469, https://doi.org/10.1039/C9RA04603H.

44. C. Yang, L. Mao, Y. Chen, et al., "Ancestral Carbonic Anhydrase With Significantly Enhanced Stability and Activity for CO_2 Capture and Utilization," *Bioresource Technology* 419 (2025): 132054, https://doi.org/10.1016/j.biortech.2025.132054.

45. J. Ge, L. Hua, and A. J. Poulose, "Thermostable Carbonic Anhydrases and Methods of Use Thereof," Patent No. US9410140B2, 2016, https://patents.google.com/patent/US9410140B2/en.

46. F. Fredslund, M. S. Borchert, J. C. N. Poulsen, et al., "Structure of a Hyperthermostable Carbonic Anhydrase Identified From an Active Hydrothermal Vent Chimney," *Enzyme and Microbial Technology* 114 (2018): 48–54, https://doi.org/10.1016/j.enzmictec.2018.03.009.

47. P. M. Doran, ed., "Homogeneous Reactions," in *Bioprocess Engineering Principles* (Academic Press, 1995), 257–296, https://doi.org/10.1016/B978-012220855-3/50011-0.

48. J. D. Cohen and H. D. Husic, "Carbonic Anhydrase Catalysed Hydrolysis of Fluorogenic Esterase Substrates," *Phytochemical Analysis* 2, no. 2 (1991): 60–64, https://doi.org/10.1002/pca.2800020203.

49. Y. Pocker and S. Sarkanen, "Carbonic Anhydrase: Structure, Catalytic Versatility, and inhibition," in *Advances in Enzymology—and Related Areas of Molecular Biology*, ed. A. Meister (John Wiley & Sons, 2006), 149–274, https://doi.org/10.1002/9780470122921.ch3.

50. K. Farzam and M. Abdullah, "Acetazolamide," in *StatPearls* (StatPearls Publishing, 2025), http://www.ncbi.nlm.nih.gov/books/NBK532282/.

51. A. Cornish-Bowden, "A Simple Graphical Method for Determining the Inhibition Constants of Mixed, Uncompetitive and Non-Competitive Inhibitors," *Biochemical Journal* 137, no. 1 (1974): 143–144, https://doi.org/10.1042/bj1370143.

52. S. Kanodia, S. Agarwal, P. Singh, S. Agarwal, P. Singh, and R. Bhatnagar, "Biochemical Characterization of Alanine Racemase- A Spore Protein Produced by *Bacillus anthracis*," *BMB Reports* 42, no. 1 (2009): 47–52, https://doi.org/10.5483/BMBRep.2009.42.1.047.

53. S. Del Prete, D. Vullo, V. De Luca, C. T. Supuran, and C. Capasso, "Biochemical Characterization of the δ-Carbonic Anhydrase From the Marine Diatom *Thalassiosira weissflogii*, TweCA," *Journal of Enzyme Inhibition and Medicinal Chemistry* 29, no. 6 (2014): 906–911, https://doi.org/10.3109/14756366.2013.868599.

54. S. R. Lotlikar, S. Hnatusko, N. E. Dickenson, S. P. Choudhari, W. L. Picking, and M. A. Patrauchan, "Three Functional β-Carbonic Anhydrases in *Pseudomonas aeruginosa* PAO1: Role in Survival in Ambient Air," *Microbiology* 159, no. Pt_8 (2013): 1748–1759, https://doi.org/10.1099/mic.0.066357-0.

55. N. R. Uda, V. Seibert, F. Stenner-Liewen, et al., "Esterase Activity of Carbonic Anhydrases Serves as Surrogate for Selecting Antibodies Blocking Hydratase Activity," *Journal of Enzyme Inhibition and Medicinal Chemistry* 30, no. 6 (2015): 955–960, https://doi.org/10.3109/14756366.2014.1001754.

Supporting Information

Additional supporting information can be found online in the Supporting Information section.

Supporting Information file 1: ansa70091-sup-0001-SuppMat.docx